Melting and Crystallization Behaviors of Isotactic Polypropylene/Acrylonitrile–Butadiene Rubber Blends in the Presence and Absence of Compatibilizers and Fillers

Aju Joseph,[1] Snoopy George,[2] Kuruvilla Joseph,[1] Sabu Thomas[2]

[1]*St. Berchmans' College, Changanacherry, Kerala, India*
[2]*School of Chemical Sciences, Mahatma Gandhi University, Kottayam, Kerala 686560, India*

Received 15 November 2005; accepted 21 December 2005
DOI 10.1002/app.23986
Published online in Wiley InterScience (www.interscience.wiley.com).

ABSTRACT: The melting and crystallization behaviors of isotactic polypropylene (PP)/acrylonitrile–butadiene rubber (NBR) blends were investigated with differential scanning calorimetry. The samples were scanned at a heating rate of 20°C/min in a nitrogen atmosphere. The effects of blend ratio, compatibilizer, and filler addition on the melting and crystallization characteristics of the blends were analyzed. Analysis showed that blend ratio had a predominant effect on the values of onset of crystallization and crystallization temperature, although the heat of fusion (ΔH_f), onset of melting, and melting temperature were unaffected. The presence of compatibilizer in the blend had an appreciable influence on the crystallization behavior. ΔH_f, heat of crystallization, and percentage crystallinity of the compatibilized blends were higher than those of the uncompatibilized blends. Fillers had little impact on the melting behavior of the blends. The morphology of the blends were analyzed with scanning electron microscopy. Hot-stage polarizing optical microscopy was used to study the spherulitic morphology of PP on the addition of NBR. The addition of a few percentage NBR significantly reduced the average spherulite size of PP in the blend followed by a marginal decrease. Blend ratio had a pronounced impact on the growth rate of PP spherulites. © 2006 Wiley Periodicals, Inc. J Appl Polym Sci 102: 2067–2080, 2006

Key words: blends; compatibilization; crystallization; morphology; spherulites

INTRODUCTION

Thermoplastic elastomers (TPEs) are an important class of materials due to their excellent rubbery properties, easy thermoplastic processability, and economic advantages.[1–5] TPEs can be block copolymers (styrene isoprene styrene [SIS], styrene butadiene styrene [SBS], polyurethanes) or blends of semicrystalline thermoplastic and rubber. These materials possess the very good physical properties of elastomers and the excellent processing characteristics of thermoplastics and thereby bridge the gap between conventional elastomers and thermoplastics. Among the various types of TPEs, those prepared by the melt mixing of a crystalline thermoplastic material and elastomers under high shearing action have gained considerable attention due to their simple method of preparation and easy attainment of desired physical properties by the variation of blend ratios. The topic of TPEs from rubber/plastic blends have been extensively covered in the literature for the last 20 years.[6–14] However, most of the TPEs have been found to be incompatible due to poor interfacial interaction between the homopolymers. Very often the incompatible blends exhibit poor mechanical properties. In such cases, it is necessary to compatibilize these blends to control the morphology for better mechanical properties. Usually, compatibilization can be accomplished by the addition of presynthesized block or graft copolymers (physical compatibilization) or by the *in situ* generation of copolymers at the interface by interfacial chemical reaction (reactive compatibilization).[15–18] The addition of a suitably selected compatibilizer for binary immiscible blends should (1) reduce the interfacial energy between the phases, (2) permit a finer dispersion during mixing, (3) provide a measure of stability against gross segregation, and (4) result in improved interfacial adhesion. The effect of the addition of block or graft copolymers as compatibilizers in binary polymer blends has been extensively reported in the literature.[19–26] In recent years, a reactive route technique has been adopted by several researchers in a large number of blend systems because it is a fast, easy, and cost-effective alternative.[27–33]

It is well documented in the literature that the crystallization of polymers in bulk usually proceeds by nucleation-controlled spherulitic growth.[34–38] Spherulites are morphological entities that consist of a large number of lamellar crystallites with well-defined boundaries radiating in all directions from one point.

Correspondence to: S. Thomas (sabut@sancharnet.in or sabut552001@yahoo.com).

Because spherulites can be easily resolved with polarized light on account of their strong birefringence, light scattering[39,40] and, particularly, hot-stage optical microscopy[41–47] have been largely used to study this phenomenon. Corresponding circular birefringent areas usually involve a dark maltese cross with arms parallel and perpendicular to the direction of polarization. It has been shown that differences in the spherulitic texture in polymeric materials depend on many factors, including the chemical structure, molecular weight, molecular weight distribution, crystallization conditions, and structural regularities in the molecule.[48] Studies have also been reported on the measurements of the spherulitic growth rate performed during isothermal crystallization with different degrees of undercooling.[49]

Growth rate are often measured by the following of the radial expansion of spherulites in the melt. In the case of an A/B miscible polymer blend where A is semicrystalline and B is amorphous, it is well-known that the growth rate of A decreases with the addition of B. In fact, at a given temperature, the decrease is directly proportional to the reduction in concentration of A in the mixture and is further decreased by an additional entropy contribution due to the presence of B. However, the growth rate of A in an A/B miscible polymer blend follows essentially the same temperature dependence as in pure A.[50,51]

Blends of polypropylene (PP) and acrylonitrile–butadiene rubber (NBR) possess the hot-oil resistance properties of NBR and the excellent processibility and mechanical properties of PP. However, these blends are incompatible due to poor physical, mechanical, and chemical interactions across the phase boundaries. Therefore, to achieve good mechanical properties, these blend systems require compatibilization. The effects of phenolic-modified polypropylene (Ph-PP) and maleic-modified polypropylene (MA-PP) as compatibilizers on the properties of PP/NBR blends were investigated[52,53] in this laboratory. However, an in-depth investigation of the crystallization and melting behavior of these blends was yet to be done. It is believed that the incorporation of a second component to a crystallizing polymer may lead to one or more of the following modifications in its crystallization behavior. (1) no effect on crystallization rate or morphology, (2) the retardation of crystallization with or without a change in morphology, or (3) the prevention of crystallization at high loadings. To our knowledge, to date, no studies have been performed on the crystallization behavior of NBR/PP blends in the presence and absence of compatibilizers. In this article, we report the influence of blend composition, compatibilizer concentration and filler incorporation on the melting and crystallization behaviors of PP/NBR blends with differential scanning calorimetry (DSC).

EXPERIMENTAL

Materials

Isotactic PP (Koylene M3060) with a melt flow index of 3 g/10 min was kindly supplied by Indian Petro Chemical, Ltd. (Vadodara, India). NBR with a 32% acrylonitrile content was supplied by Synthetics and Chemicals (Bareli, Uttar Pradesh, India).

Preparation of the compatibilizers

MA-PP was prepared by the melt mixing of PP with maleic anhydride (5 wt %), benzoquinone (0.75 wt %), and dicumyl peroxide (3 wt %) in a Brabender plasticoder (model PLE-330; Cleveland, OH, USA) at 180°C; the rotor speed was 60 rpm. Ph-PP was prepared by the melt mixing of PP with dimethylol phenolic resin [SP-1045 (4 parts) and stannous chloride (0.8 wt %)] at 180°C. The fillers used were high-abrasion furnace black (HAF-N 330) and silane-treated silica (TSi). TSi was prepared by the treatment of silica (Si; 100 g) with a Union Carbide A174 silane coupling agent (5 g) (Dow Chemicals, Germany).

Blend preparation

PP/NBR blends were prepared by the melt mixing of PP with NBR in a Brabender plasticoder at 180°C. The rotor speed was optimized as 60 rpm. In the case of the uncompatibilized blend, PP was first melted for 2 min and then NBR was added; the mixing was continued for another 6 min. In the case of the compatibilized blends, the compatibilizer was added to PP before the addition of NBR. The compatibilizer concentration was varied from 1 to 15 wt %. The uncompatibilized blends were designated as P_{100}, P_{85}, P_{70}, P_{50}, and P_{30} where the subscripts denote the weight percentage of PP in the blend. The Ph-PP and MA-PP compatibilized PP/NBR blends were designated as PP_{70x} and PM_{70x}, respectively, where x denotes the weight percentage of compatibilizer in the blend. The filled PP/NBR blends were prepared with different fillers, namely, carbon black (C), Si, and TSi. The filled blends were designated as $P_{50}C_{30}$, $P_{50}Si_{30}$, and $P_{50}TSi_{30}$ for C-, Si-, and TSi-filled blends, respectively, where 30 denotes the weight percentage of filler in the blend. In the case of filled blends, the amount of filler was taken with reference to the rubber phase, that is, NBR. The amount of filler was always 30 wt % with respect to the rubber phase.

DSC analysis

A PerkinElmer DSC-7 apparatus (Wellesley, MA, USA) was used to determine the melting and crystallization behaviors of the PP and PP/NBR blends. The following conditions were applied for the study of the melting and crystallization behaviors:

Stage 1: The heating of the sample in the calorimeter at a rate of 20°C/min from 20 to 210°C.
Stage 2: Isothermal annealing at 210°C for 5 min; this was done to remove any crystalline nuclei.
Stage 3: The cooling of the sample in the calorimeter to 20°C at a rate of 20°C/min.
Stage 4: The heating of the sample in the calorimeter again to 210°C at a rate of 20°C/min.

From the heating and cooling curves, the melting and crystallization parameters were estimated. These included

1. Temperature at the onset of melting ($T_{m,\text{onset}}$).
2. Melting temperature (T_m).
3. Temperature at the onset of crystallization ($T_{c,\text{onset}}$).
4. Crystallization temperature (T_c).
5. Temperature at the endset of crystallization ($T_{c,\text{endset}}$).
6. Normalized value of heat of fusion (ΔH_f).
7. Normalized value of heat of crystallization (ΔH_c).
8. Percentage crystallinity (X_c).

X_c was calculated with the following expression:

$$X_c = \Delta H_f \times 100/\Delta H_f^0 \quad (1)$$

where ΔH_f is the heat of fusion of the sample and ΔH^0_f is the heat of fusion of 100% pure crystalline PP, which was taken as 209 J/g.[54,55]

Hot-stage optical microscopy

The optical hot-stage experiments were conducted with a Leica hot-stage system (Westler, Germany) with a programmed temperature controller and cooling system. The hot stage was mounted on a Leica DMLP microscopy system equipped with a 20× objective (magnification = 200×) and a Carton charged coupling device camera (Tokyo, Japan) (http://www.carton-opt.co.jp). The optical photographs were recorded with cross-polarized light at intervals of 5 min and analyzed with Scalar Impressive Work software (Tokyo, Japan). Spherulite diameter was measured on freshly prepared films to avoid degradation. A compression-molded thin film was placed on a microscope glass slide, and a thin cover glass was put on the top of it. The resulting sandwich was then inserted in the hot stage at room temperature and heated to 200°C at a heating rate of 20°C/min. The sample was annealed at 200°C for 5 min; it was then cooled to its T_c (124°C) at a rate of 20°C/min. At 124°C, spherulite growth started. The spherulite growth was followed isothermally as a function of time. The radius was then plotted as a function of time, and the initial slope of this line was calculated. This was the average radial growth rate. All samples were measured in transmission mode with a bright field and crossed polars. The film thickness was kept around 40 ± 5 μm. For each sample, nearly 80 spherulites were considered for diameter measurements.

RESULTS AND DISCUSSION

Uncompatibilized blends: Effect of blend ratio

Melting behavior

The melting of the PP/NBR blends was studied with DSC. From the heating curves shown in Figure 1, $T_{m,\text{onset}}$, T_m, ΔH_f, and X_c were computed. The melting behavior of PP in all of the blends is given in Table I. $T_{m,\text{onset}}$ and T_m of virgin PP were 140 and 164°C, respectively. X_c of neat PP was 42.8%. Both $T_{m,\text{onset}}$ and T_m of PP were not affected by blending. The variation of X_c of PP as a function of blend composition is shown in Figure 2. X_c of PP remained almost unaffected by the addition of NBR. This indicated a lack of interaction of the PP and NBR phases. The behavior was very analogous to the behavior of incompatible blends. The two-phase character of the blend was evident from the morphology given in the latter part of the article.

Crystallization behavior

The crystallization behavior of neat PP can be evaluated from the cooling curves given in Figure 3. Shown in Figure 3 are the $T_{c,\text{onset}}$, T_c, and ΔH_c; the values were 118°C, 104°C, and 88.8 J/g, respectively. Both $T_{c,\text{onset}}$ and T_c of PP increased with increasing rubber concentration in the blend. T_c and $T_{c,\text{onset}}$ of PP were increased by 10°C with the incorporation of

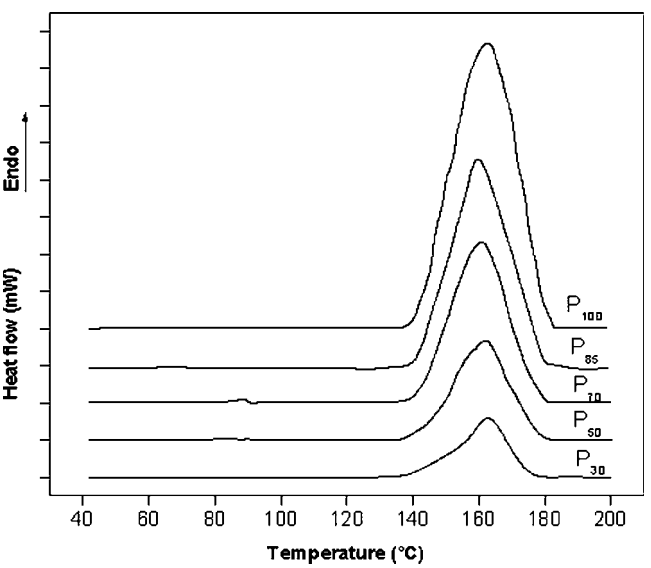

Figure 1 DSC heating curves of PP_{100} and its modified blends.

TABLE I
Melting and Crystallization Behaviors of PP/NBR Blends and Their Filled Systems

Sample	$T_{m,\text{onset}}$ (°C)	T_m (°C)	$T_{m,\text{endset}}$ (°C)	ΔH_f	X_c
P_{100}	140	164	180	89.4	42.8
P_{85}	140	160	179	89.8	43
P_{70}	139	162	180	89.3	42.7
P_{50}	137	164	179	91.7	43.9
P_{30}	138	164	177	89.8	43
PP_{7001}	139	162	175	89.2	42.7
PP_{7005}	138	179	185	92.1	44.1
PP_{7010}	137	180	184	92.7	44.4
PM_{7001}	138	163	182	91.7	43.9
PM_{7005}	137	169	183	93.8	44.9
PM_{7010}	137	172	183	95.6	45.7
$P_{50}Si_{30}$	137	166	172	90.3	43.2
$P_{50}TSi_{30}$	138	168	173	91.8	43.9
$P_{50}C_{50}$	135	167	174	92.7	44.4

$T_{m,\text{endset}}$ = temperature at which melting ceases.

70 wt % rubber. However, ΔH_c of PP was not affected by blending.

Effect of reactive compatibilization

Before we discuss the role of the compatibilizers on the morphology, it is important to discuss the morphology of uncompatibilized blends. The morphology of the uncompatibilized blends of PP and NBR is presented in Figure 4. The PP-rich blends (i.e., P_{70}) exhibited a matrix/droplet-type morphology, where PP formed the matrix and NBR was dispersed as coarse domains. With increasing concentration of the NBR phase, the size of the dispersed NBR phases increased, as seen from the micrograph of P_{50} shown in Figure 4(b). The blend P_{30} possessed a typical cocontinuous morphology, where the PP and NBR phases formed an interpenetrating cocontinuous structure.

As mentioned earlier, the addition of a suitable compatibilizer often reduces the interfacial energy of the phases, permits finer dispersion during mixing, provides a measure of stability against gross phase segregation, and results in improved interfacial adhesion. It is widely recognized that in polymer blends, the physical properties are affected by the resulting morphology of the compatibilized blends. In this study, two compatibilizers were used for the interfacial modifications, the maleic anhydride modification of PP and the phenolic modification of PP. The mechanisms of the maleic modification of PP and the phenolic modification of PP are shown in reaction Schemes 1 and 2, respectively. The compatibilizing action of MA-PP was due to the dipolar interaction between the maleic anhydride group of MA-PP and the nitrile group of NBR. Figure 5(a–d) represents blends containing 1, 5, 10, and 15% MA-PP, respectively. The size of the dispersed NBR phase decreased with the addition of the MA-PP. This reduction in particle size with the addition of MA-PP was due to the reduction in interfacial tension between the dispersed NBR and the PP matrix and also the suppression of coalescence.

When PP was melt-mixed with dimethylol phenolic resin and $SnCl_2$, dimethylol groups were grafted on to the PP backbone chain, as shown in reaction Scheme 2. When Ph-PP was added to the PP/NBR blend, there was the possibility for the formation of a graft copolymer between PP and NBR, as shown in reaction Scheme 2. This graft copolymer acted as an interfacial emulsifier and thus reduced interfacial tension and coalescence and led to a small and uniform distribution of the NBR phase, as seen in the SEM micrographs given in Figure 6(a–d). The average domain sizes of the compatibilized blends were analyzed as a function of compatibilizer concentration, as shown in Figure 7. The number-average domain size of the unmodified blend was 5.87 μm. The addition of 1% MA-PP caused a domain size reduction of 35%. The further addition of MA-PP did not change the domain size considerably; a leveling off was observed. In the case of Ph-PP compatibilized blends, the average diameter of the dispersed NBR phase decreased up to the addition of 10 wt % Ph-PP, where the domain size was reduced by 77% of the domain size of the unmodified blend. However, the further addition of the compatibilizer increased the domain size. The domain size distribution curves for the Ph-PP and MA-PP compatibilized blends are shown in Figures 8 and 9, respectively. In the case of the unmodified blend, a high degree of polydispersity was evident by the large width of the distribu-

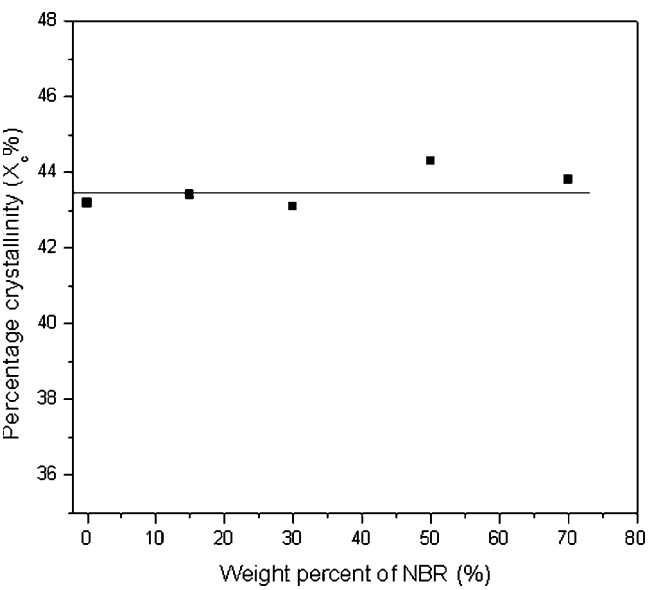

Figure 2 Change in crystallinity of PP with the addition of NBR.

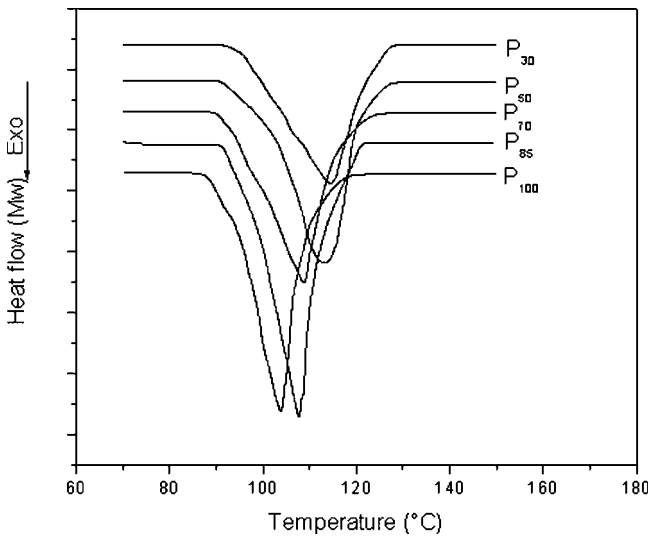

Figure 3 DSC cooling curves of P_{100}, P_{85}, P_{70}, P_{50}, and P_{30}.

tion curve. With increasing concentration of the compatibilizer (Ph-PP and MA-PP), the polydispersity decreased, as evidenced by the decrease in the width of the distribution curve. In the case of the Ph-PP compatibilized blend, a narrow distribution was obtained with the addition 10% Ph-PP. The equilibrium concentration at which the domain size leveled off or increased was considered the critical micelle concentration due to the so-called interfacial saturation, which was discussed extensively in our earlier publications.[3,52,53] Interestingly, a bimodal distribution was achieved in the case of Ph-PP compatibilized blends. This was due to the very efficient compatibilization action of Ph-PP due to the formation of the copolymer at the interphase, as shown in Scheme 2.

Melting behavior

The melting behavior of the compatibilized PP/NBR blends obtained from the heating curves (Fig. 10) is

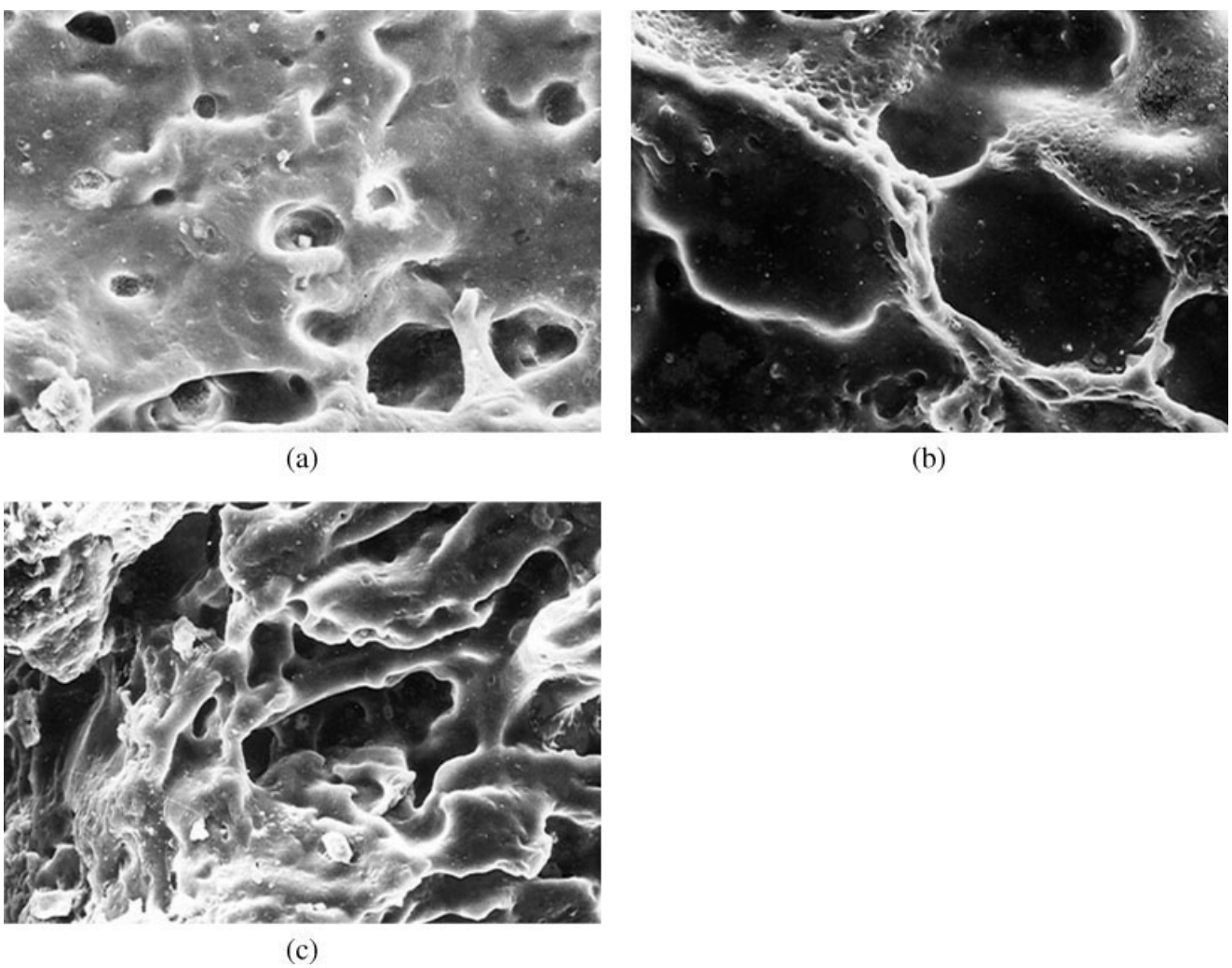

Figure 4 Scanning electron micrograph of (a) P_{70}, (b) P_{50}, and (c) P_{70} blend.

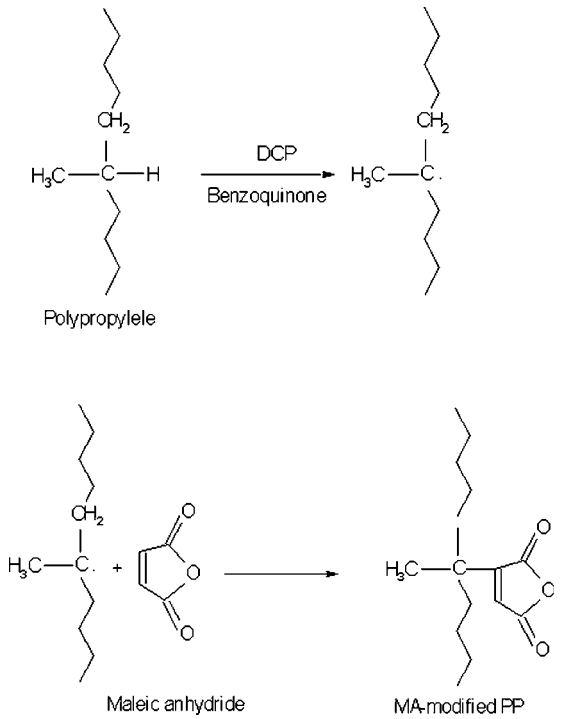

Scheme 1 Reaction pathway for the maleic anhydride modification of PP.

presented in Table I. The addition of compatibilizers (5 wt %) increased T_m of PP appreciably. This may have been due to the restriction in the movement of the macromolecule developed from the better interaction from compatibilization. It is important to note that 5 wt % of compatibilizer was necessary to alter the melting behavior. Beyond 5 wt % compatibilizer, T_m of PP was affected little. Similarly, ΔH_f of PP also increased slightly in the presence of 5 wt % compatibilizer. X_c of PP in the crystallized blend given in Table I reveals that compatibilization did not affect the crystallinity of the blend.

Crystallization behavior

The crystallization characteristics of PP in compatibilized blends derived from cooling curves given in Figure 11 are listed in Table II. The addition of 1% PP-MA and Ph-PP compatibilizers significantly reduced the T_c of PP in the blend, whereas the ΔH_c values were only marginally affected.

In summary, from the melting and crystallization behaviors of the compatibilized blends, we concluded that the presence of compatibilizer influenced the melting and crystallization characteristics of PP in PP/NBR blends. This was not unexpected and was due to the fact that the compatibilizer enhanced the interfacial interactions between the phases in the blends. This, indeed, affected the crystal formation because the amorphous NBR phase may have been present at the interspherulite region of PP. The enhancement of interfacial properties of the blends in the presence of compatibilizer was evident from the morphology of the compatibilized blends demonstrated in Figures 5 and 6. Compatibilizer drastically decreased the dispersed particle size by diminishing the interfacial tension between the component polymers and suppressing the coalescence phenomena. It has already been reported that addition of compatibilizer can increase interfacial interaction. Because of the increased interaction, the impurities present in the rubber phase can migrate to the PP phase. This can affect the crystallization process. However, a critical concentration of the compatibilizer is needed to produce changes in the melting and crystallization process.

For example, in the case of crystallization process, T_c was shifted remarkably by the addition of 1% compatibilizer. With a further increase in compatibilizer, T_c increased. However, for the melting, a noticeable change was observed only at 5 wt % compatibilizer. Further experiments are needed to understand this phenomenon.

Effect of filler addition

Fillers are extensively used in TPEs for property modification, cost reduction, and improvements in the processability. However, the effect of fillers on the crystallization of TPEs has not been reported. As shown in Tables I and II, the fillers did not affect the melting and crystallization behaviors of the blend. Table I presents the melting characteristics of PP in blends in the presence of three different fillers; these fillers had no significant impact on the melting behavior. Furthermore, filler addition did not affect the ΔH_f values of PP in the blends.

Isothermal crystallization

The measurement of the radial spherulite growth rate of PP in PP/NBR blend was followed at isothermal crystallizations conditions with a polarizing optical microscope coupled with a hot stage. Figure 12(a–f) demonstrates the different stages of the spherulitic growth of neat PP. The micrographs were taken at intervals of 5 min. Figure 12(a) shows the very beginning of spherulite growth. Previously, this sample was kept at 200°C for 5 min to destroy any crystallites present in the system. It was then cooled to its T_c at a cooling rate of 20°C/min. Figure 12(b) shows the spherulite after 6 min of annealing at T_c. In Figure 12(c,d), one can see the change in size of PP spherulites, which were captured at 5 min intervals. Figure 12(f) shows the spherulite just before the completion of crystallization process. In the case of neat PP, the final spherulitic diameters ranged from about 130 to

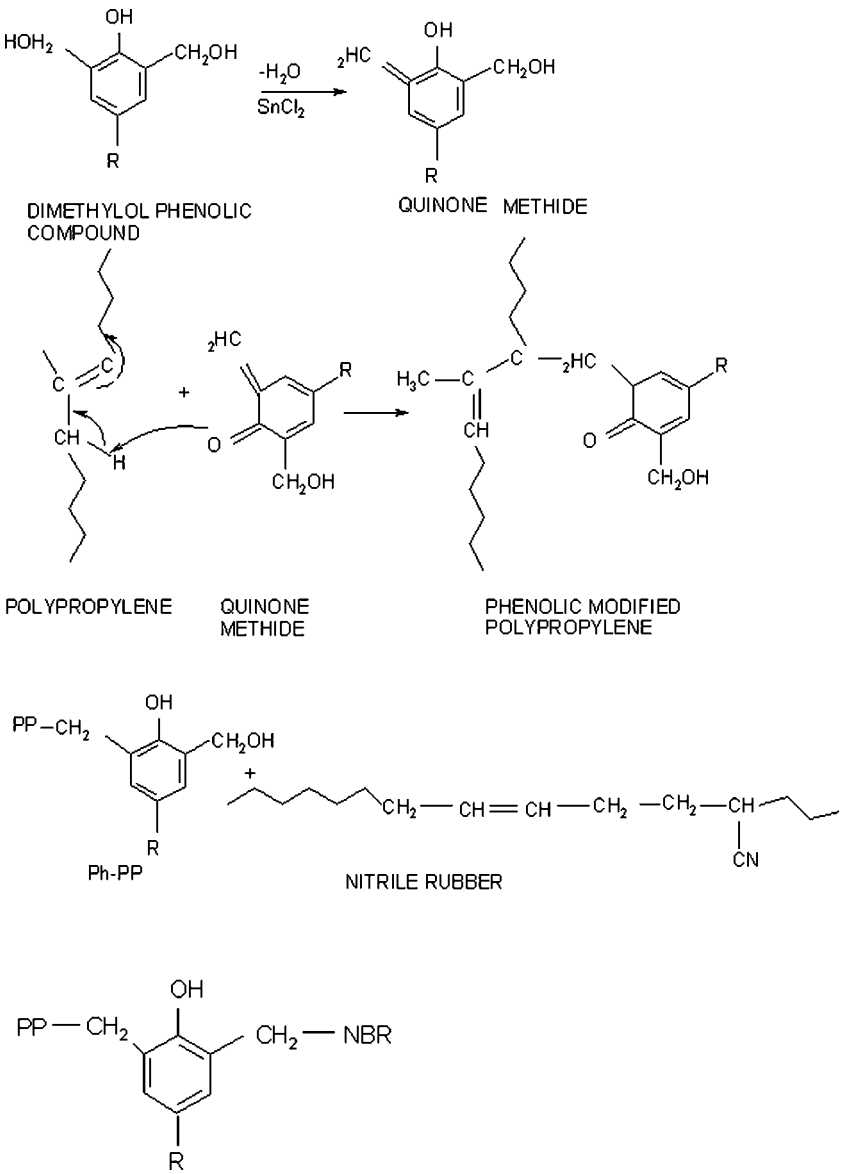

Scheme 2 Reaction pathway for the dimethylol phenolic modification of PP.

60 μm. This depended on the number of nuclei per unit area present during the crystallization conditions at T_c. The nucleation in PP may have been due to the self-nucleation process or nucleation due to foreign substances present in the polymer melt.

Figure 13(a–d) illustrates the effect of the addition of the amorphous NBR phase on the spherulitic growth of PP. The graphical representation of the influence of the rubber content on the spherulite diameter of PP is shown in Figure 14. The decrease in spherulite diameter could have been due to the greater nucleation induced by rubber phase in the intraspherulitic and interspherulitic regions. Interestingly, the incorporation of 1 wt % NBR reduced the average spherulitic diameter from 125 to 72 μm. The size reduction may have been due to the greater nucleation in the presence of amorphous phase. It may also have been due to the NBR droplets present at the interspherultic and intraspherulitic regions, which may have hindered the growth of spherulites. The dispersed amorphous phase was assumed to be uniformly distributed in the melt in droplet-like domains even after the melting. The crystallizable PP component formed the matrix phase in the blend at the lower rubber content. Therefore, nucleation could have occurred due to the presence of rubber particles (heterogeneous nucleation). At the same time, more nuclei were activated, and more growth centers were formed. This increased the number of spherulites and, hence, reduced the radius of the final spherulite.

The average spherulitic diameter of blends containing 10 wt % (regime I in Fig. 14) NBR was 84 μm. At 30 wt % NBR, the diameter was reduced to 80 μm. In short, the polarizing optical microscopy studies revealed that the presence of NBR in the PP matrix

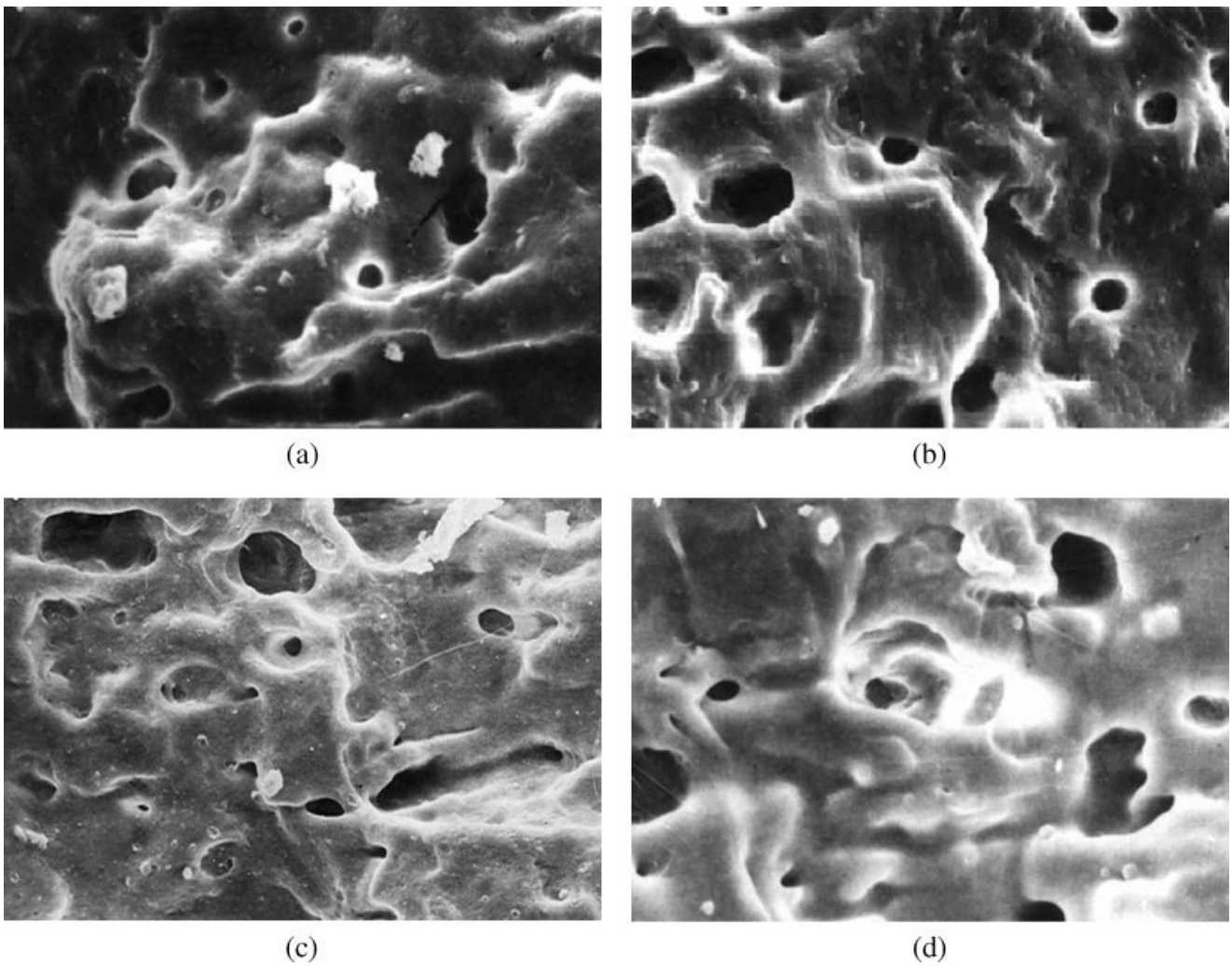

Figure 5 Scanning electron micrographs of P_{70} blends compatibilized with (a) 3, (b) 7.5, (c) 10, and (d) 15% Ph-PP.

had a significant impact on the spherulite diameter of PP but only at very low and very high concentrations of NBR. This was due to the fact that at very low concentrations of NBR in PP, energy was required to effect the rejection of the second component. However, at higher concentrations of the NBR phase, rubber particles coalesced together to form a large agglomerate, and the growing spherulite had to engulf the big domains of NBR (regime II in Fig. 14) When the rubber content was higher than 50%, it became a continuous phase, and the diameter was further reduced (regime III).

Even 1 wt % NBR [Fig. 13(a)] had a tremendous impact on spherulitic growth. Radial growth of the PP spherulite as a function of time is shown in Figure 15 for neat PP and the blends. It has been shown that the presence of foreign inclusions in the melt, as in the case of immiscible blends, can disturb the crystallizing front.[53,56] These rubber domains could impart nucleation at a very low concentration of NBR (up to 10 wt %). This is shown in regime I in Figure 16. However, as the size increased (20 $\leqslant$ wt % of NBR $\leqslant$ 40), the mechanism may have changed. This is shown as regime II in Figure 16. Because of the growing crystal front, the dispersed rubber domains were either engulfed or got trapped within the spherulite. If there were interfacial interactions between the blend components, the growing crystal front had to work against the dispersed phase in the melt. In the case of a one-phase melt, some energy is required to affect the rejection of the second component from the crystallizing polymer. In the case of a two-phase melt, where the second component has taken the form of droplet-like domains, energy must also be dissipated for the rejection, engulfment, and/or deformation of the second component. These energy dissipations constitute energy barriers, which influence the growth rate of the spherulite in the melt. Bartczak, Galeski, Martuscelli, and coworkers[57,58] modified the classical Fischer–Turnbull equation to account for the energy dissipations that result during the crystallization of a polymer in the presence of

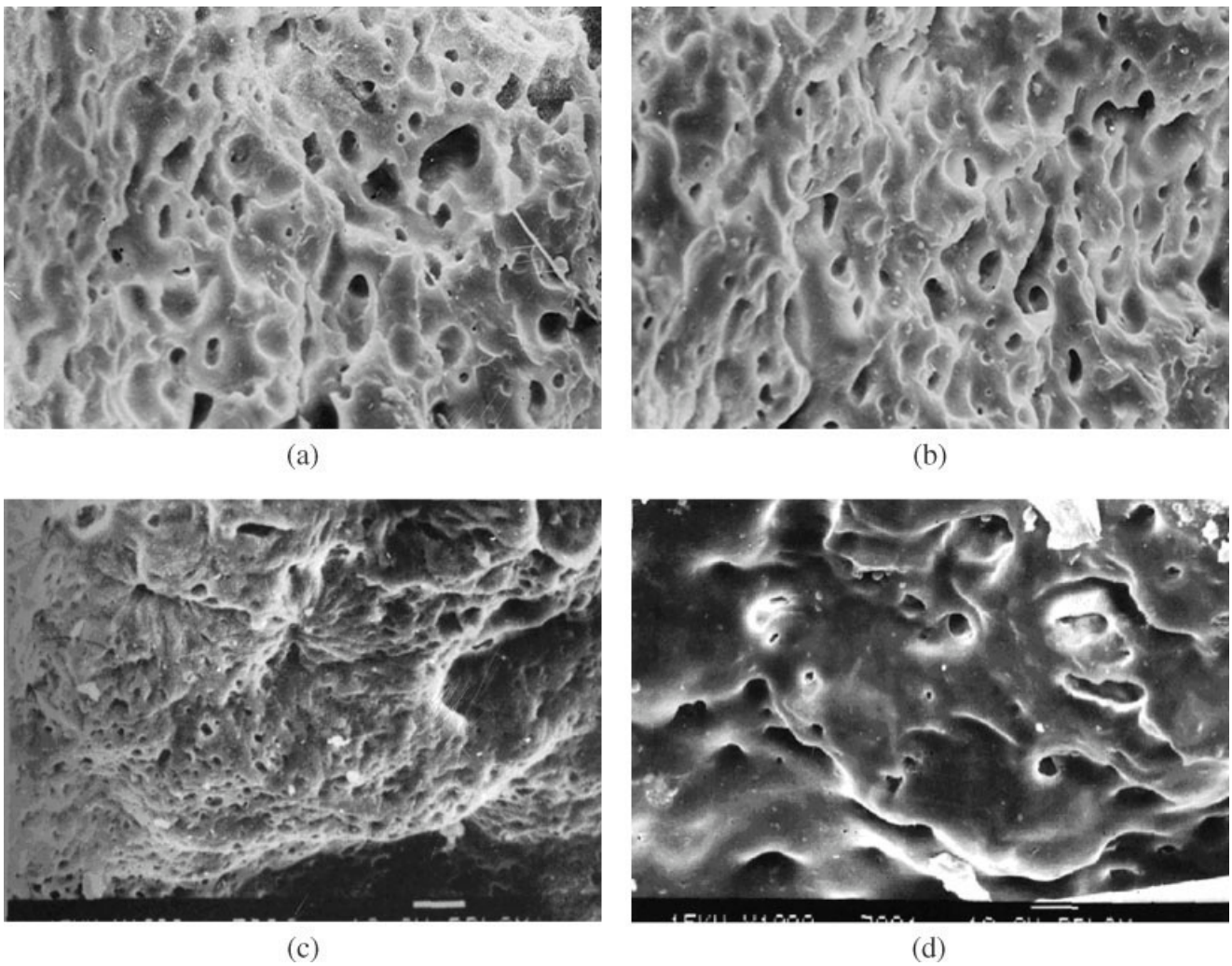

Figure 6 Scanning electron micrographs of P_{70} blends compatibilized with (a) 3, (b) 7.5, (c) 10, and (d) 15% MA-PP.

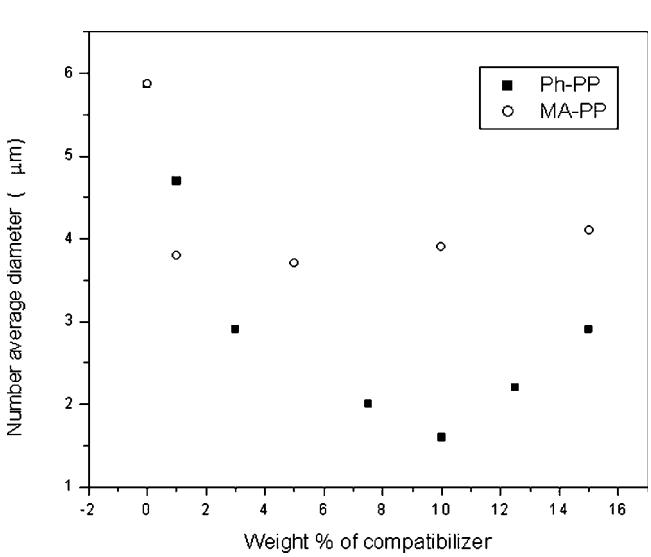

Figure 7 Effect of Ph-PP and MA-PP compatibilizer concentration on the domain size of the dispersed phase of P_{70}.

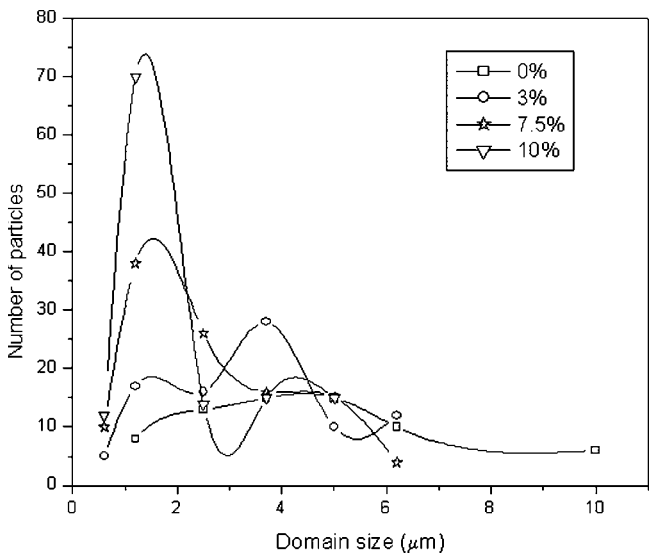

Figure 8 Effect of Ph-PP compatibilizer concentration on the domain size distribution of the dispersed phase of P_{70}.

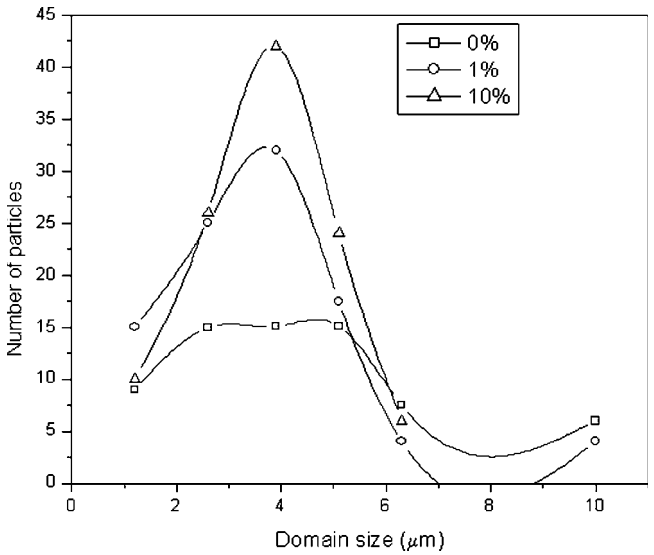

Figure 9 Effect of MA-PP compatibilizer concentration on the domain size distribution of the dispersed phase of P_{70}.

noncrystallizing spherical domains. The modified equation is

$$G = G_0 \exp(-E_{D*}/\kappa T) \exp(-\Delta\phi^*/\kappa T) \times \exp[-(E_1 + E_2 + E_3 + E_4 + E_5)/\kappa T] \quad (2)$$

where the term $\exp(-E_{D^*}/\kappa T)$ is referred to as the transport term, $\exp(-\Delta\phi^*/\kappa T)$ is referred to as the nucleation term, G is the growth rate, and G_0 is the pre-exponentional term. E_1 is the energy dissipated by the crystal to affect the rejection of the second component into the interlamellar regions, E_2 is the energy dissipated by the spherulite front to affect the rejection of the droplet-like domains in the melt, E_3 is the kinetic energy required to overcome the inertia of the drops, E_4 is the energy required to form new interfaces between the spherulite and the drop when engulfment occurs, and E_5 is the energy dissipated when the engulfed drops are deformed by the crystallizing front. The crystallization of polymer blends whose components are phase-separated in the melt is influenced by both the size of the dispersed phase and the interfacial energies.[59,60] The radial growth rate of PP spherulite as a function of rubber addition is shown in Figure 15. The driving force for the rejection, engulfment, and/or deformation process lies in the difference of the interfacial free energy between the crystallizing front and inclusions (γ_{ps}) and the interfacial free energy between the melt and inclusions (γ_{pi}):

$$\Delta F = \gamma_p - \gamma_{pi} \quad (3)$$

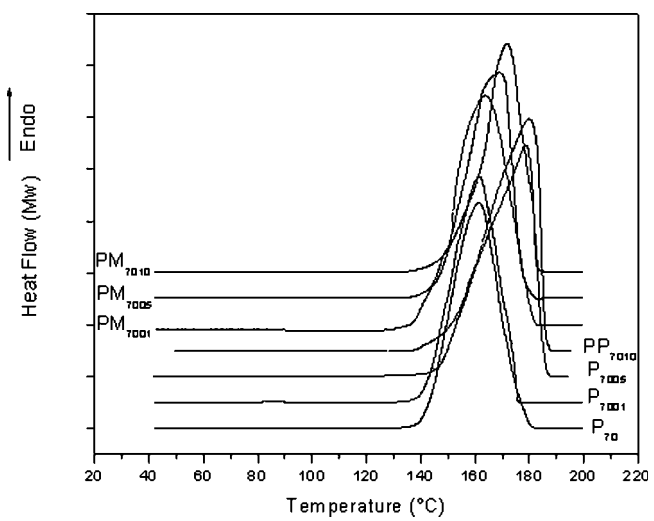

Figure 10 DSC heating curves of P_{70} and its modified blends.

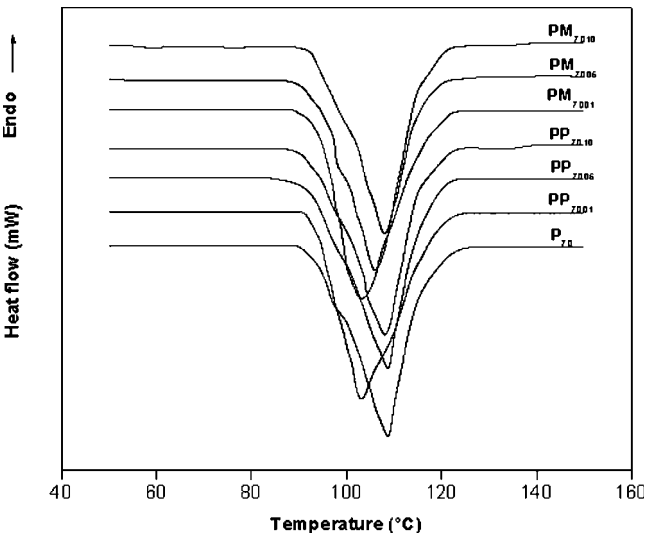

Figure 11 DSC cooling curves of PP_{70} and its modified samples.

TABLE II
Crystallization Characteristics of PP/NBR Blends and Their Filled Systems

Sample	$T_{c,\text{onset}}$ (°C)	T_c (°C)	$T_{c,\text{endset}}$ (°C)	ΔH_c (J/g)
P_{100}	118	104	88	88.8
P_{85}	121	108	91	92
P_{70}	125	109	90	92.4
P_{50}	127	114	91	92
P_{30}	127.4	114.5	92	93
PP_{7001}	122	102.5	92	90.7
PP_{7005}	121.5	109	87	91.7
PP_{7010}	124	108	88	92.5
PM_{7001}	122	103	89	91.8
PM_{7005}	123	106	88	93.2
PM_{7010}	121	108	92	95
$P_{50}Si_{30}$	128	114	94	88.8
$P_{50}TSi_{30}$	131	114	91	90.9
$P_{50}C_{50}$	126	114	94	93.3

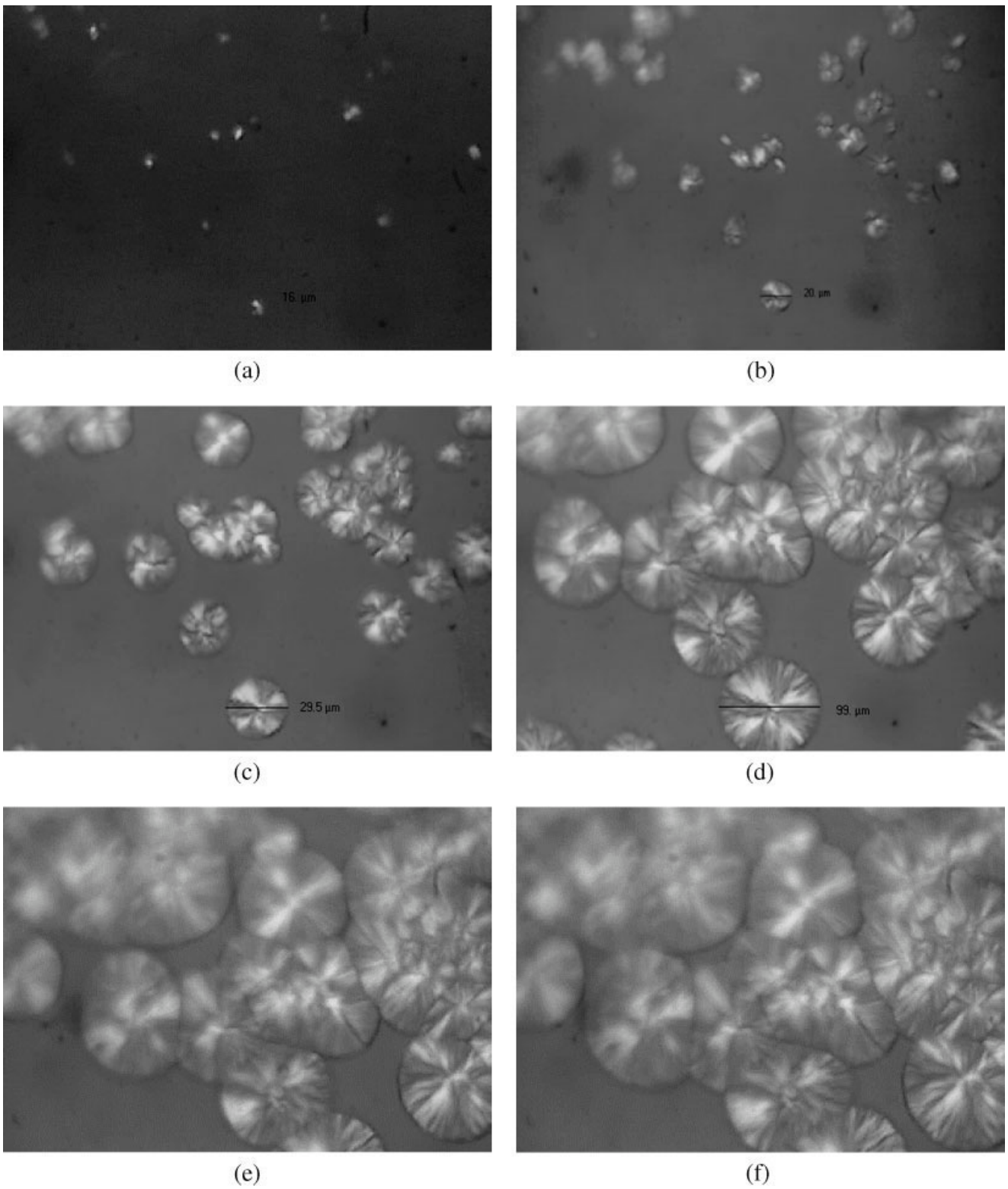

Figure 12 Polarized optical photomicrographs of the different stages of spherulite growth in pure PP. (All of these photographs were taken in the transmission mode with cross-polarized light at 200× magnification.) (a) Taken 1 min after the spherulite growth started. All other micrographs were taken at an interwell of 5 min.

For $\Delta F < 0$, the dispersed domains in the melt are more likely to be engulfed than rejected by the growing front.

However, when $\Delta F > 0$, the situation was more complicated. At slow rates of crystallization, the domains were pushed along by the growing front

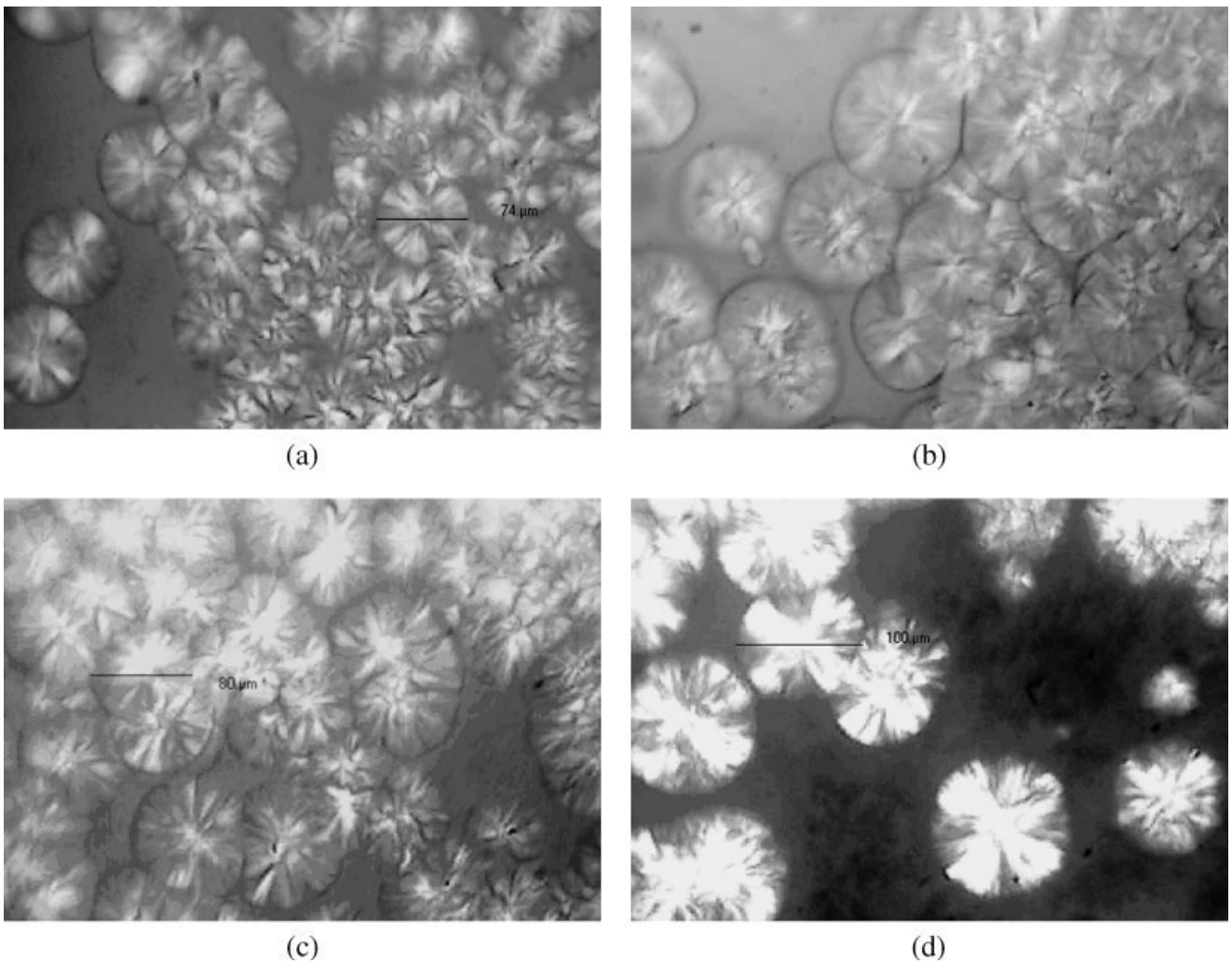

Figure 13 Polarized optical micrographs of blends of PP and NBR (all of these photographs were taken in the transmission mode with cross-polarized light) blends (magnification = 200×) (a) 1, (b) 2, (c) 6, and (d) 10 wt % NBR.

(regime I in Figs. 15 and 16), whereas at higher rates, they were simply engulfed, as shown in regime II in Figure 16. At some intermediate state, the domains may have been pushed for short distances before they were engulfed by the crystallizing front. Engulfment occurred when the viscous hindrance caused by the motion of the domains overwhelmed the forces of repulsion. This implied a critical rate at which the pushing of the domains no longer occurred and engulfment took precedence. With these arguments, for a given ΔF, there must be a critical domain size such that at a constant growth rate, domains of the size or larger are simply engulfed and no longer pushed by the front. Engulfment occurs above this critical size because the hydrodynamic force is proportional to the domain size, whereas the repulsive are determined by the factors such as shape of the interface behind the particle. The critical size itself is dependent on the system,

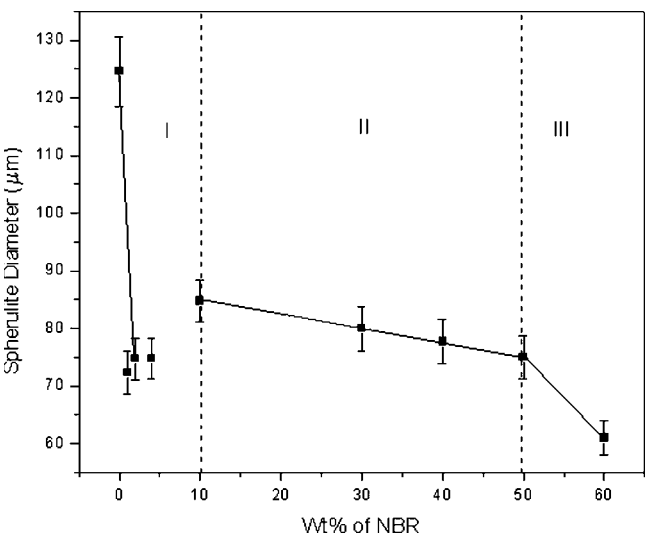

Figure 14 Spherulite diameter in the PP/NBR blends.

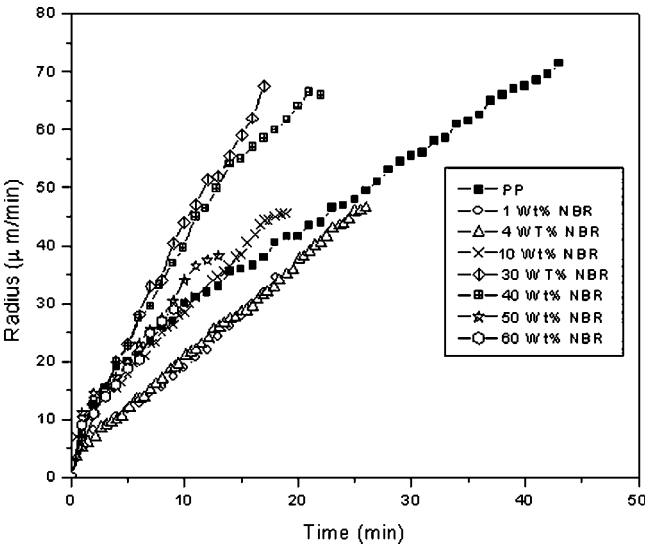

Figure 15 Radial growth of the PP spherulite as a function of time.

that is, on the interfacial energies, viscosities, and heat conductivities. The growing crystals have to change their path to reject or engulf the dispersed particles. This will lead to the reduction in the spherulite diameter. These droplet-like domains remaining in the path of the crystallizing growth front markedly hinder the spherulite growth, and hence, the addition of rubber decreases the spherulitic diameter. As shown in Figure 16, the incorporation of a small amount of rubber, up to 10 wt % NBR, decreased the growth rate significantly. This was due to the fact that at a low concentration of rubber, the rubber particles were pushed by the growing front (regime I). As the amount of rubber increased, the domain size increased; therefore, the rubber particles were engulfed (regime II). This resulted in a slight increase in the growth rate. As the amount of rubber further increased, the rubber became a continuous phase. This caused a decrease in the growth rate (regime III).

CONCLUSIONS

The melting and crystallization behaviors of PP/NBR blends were studied with DSC and polarizing microscopy. The effects of rubber addition on T_m, $T_{c,\text{onset}}$, T_c, and X_c of PP/NBR blends were studied as a function of composition. The influence of compatibilization and filler addition on these parameters were also studied. The blend ratio had no significant effect on the melting process. X_c was unaffected by blend ratio and filler addition. T_c of PP increased with increasing concentration of the NBR phase.

The addition of PP-Ma and Ph-PP compatibilizers permitted finer dispersion, provided a measure of stability against gross phase segregation, and resulted in improved interfacial adhesion. The compatibilizing action of MA-PP was due to the dipolar interaction between the maleic anhydride group of MA-PP and the nitrile group of NBR. This reduction in particle size with the addition of MA-PP was due to the reduction in interfacial tension between the dispersed NBR and PP matrix and also the suppression of coalescence. The addition of Ph-PP into the PP/NBR blend led to the formation of a graft copolymer between PP and NBR. This graft copolymer acted as an interfacial emulsifier and thus reduced interfacial tension and coalescence and led to the small and uniform distribution of the NBR phase, as confirmed in the SEM micrographs. The efficient compatibilization action of Ph-PP due to the formation of the copolymer at the interphase gave a bimodal distribution of domains. Compatibilization had an appreciable effect on T_m and T_c of PP, and these changes could be correlated with the morphology of the blend. Filler addition did not affect the melting behavior of the blend.

The spherulite diameter in pure isotactic PP was measured as a function of time. The effect of NBR incorporation on the spherulitic diameter of PP was also measured. The incorporation of 1 wt % rubber decreased the spherulitic diameter drastically followed by a marginal effect at higher concentrations. In fact, the amorphous NBR rubber droplets in the path of the crystallizing growth front of the PP substantially hindered the spherulitie growth, and this delayed growth provided sufficient time for the activation of more nuclei; hence, the overall nucleation density increased, and the addition of rubber decreased the spherulite diameter. The size of the dispersed domains had a pronounced effect on the spherulite growth rate. At low rubber contents, the growth rate decreased up to 10 wt % NBR. This was

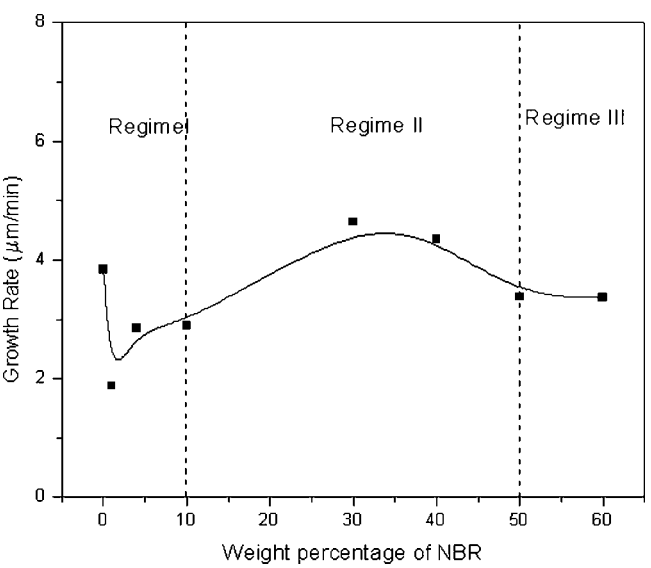

Figure 16 Radial growth rate of the PP spherulite as a function of rubber addition.

because the growing spherulite had to push the rubber domains. However, as the amount of NBR increased, the size of the dispersed domains became larger due to their coalescence, as evidenced from the morphology of the blends, and hence, the spherulitic growth rate was increased up to 40. This was because the NBR domains attained a critical domain size, and therefore, the engulfing of the rubber domains took place. The spherulite growth rate further decreased when the rubber content was more than 50%. This was due to the fact that the rubber became a continuous phase.

References

1. Thermoplastic Elastomers: A Comprehensive Review; Legge, N. R.; Holder, H. E.; Shroeder, H. E., Eds.; Hanser: Munchen, Germany, 1987.
2. De, S. K.; Bhowmich, A. K. Thermoplastic Elastomers from Rubber Plastic Blends; Ellis Horwood: Chichester, England, 1990.
3. George, S.; Ramamurthy, K.; Anand, J. S.; Groeninckx, G.; Varughese, K. T.; Thomas, S. Polymer 1999, 40, 4325.
4. Thomas, S.; Groeninckx, G. Polymer 1999, 40, 5799.
5. Oderkerk, J.; Groeninckx, G. Polymer 2002, 43, 2219.
6. Walker, R. M. Hand Book of Thermoplastic Elastomers; Van Nostrand Reinhold: New York, 1979.
7. West, J. C.; Cooper, S. L. In Science and Technology of Rubber; Eirich, F. R., Ed.; Academic: New York, 1978; Chapter 13.
8. Whelan, A.; Lee, K. S. Development in Rubber Technologies, Thermoplastic Rubbers; Applied Science: London, 1982.
9. Oderkerk, J.; de Schaetzen, G.; Goderis, B.; Hellemans, L.; Groeninckx, G. Macromolecules 2002, 35, 6623.
10. Oderkerk, J.; Groeninckx, G.; Soliman, M. Macromolecules 2002, 35, 3946.
11. Coran, A. Y.; Patel, R.; Williams, D. Rubber Chem Technol 1980, 53, 141.
12. Coran, A. Y.; Patel, R.; Williams, D. Rubber Chem Technol 1980, 53, 781.
13. Coran, A. Y.; Patel, R.; Williams, D. Rubber Chem Technol 1983, 56, 1045.
14. Coran, A. Y.; Patel, R.; Williams, D. Rubber Chem Technol 1982, 55, 1063.
15. Koning, C.; van Duin, M.; Pagnoulle, C.; Jérôme, R. Prog Polym Sci 1998, 23, 707.
16. Paul, D. R.; Bucknall, C. B. Reactive Compatibilisation; Wiley: New York, 2000; Chapter 17, p 539.
17. Aravind, I.; Albert, P.; Ranganathaiah, C.; Kurian, J. V.; Thomas, S. Polym 2004, 45, 4925.
18. Ravikumar, H. B.; Ranganathaiah, C.; Kumaraswamy, G. N.; Thomas, S. Polymer 2005, 46, 2372.
19. Fayt, R.; Jerome, R.; Teyssie, P. Polym Eng Sci 1987, 27, 328.
20. Bucknall, D. G.; Higgins, J. S.; Rostami, S. Polymer 1992, 33, 4419.
21. Thomas, S.; Prud'homme, E. Polymer 1992, 33, 4260.
22. Braun, D.; Fischer, M.; Hellmannt, G. P. Polymer 1996, 37, 3871.
23. Macoscko, C. W.; Guégan, P.; Khandpur, A. K.; Nakayama, A.; Marechal, P.; Inoue, T. Macromolecules 1996, 29, 5590.
24. Lee, M. S.; Lodge, T. P.; Macosko, C. W. Macromol Chem Phys 1998, 199, 1555.
25. Hlavatá, D.; Horák, Z.; Hromádková, J.; Lednický, F.; Pleska, A. J Polym Sci Part B: Polym Phys 1999, 37, 1647.
26. Harrats, C.; Fayt, R.; Jerôme, R. Polymer 2002, 43, 863.
27. Kim, S.; Kim, J. K.; Park, C. E. Polymer 1997, 38, 1809.
28. Dedecker, K.; Groeninckx, G. Macromolecules 1999, 32, 2472.
29. John, B.; Varughese, K. T.; Oomen, Z.; Pötscheke, P.; Thomas, S. J Appl Polym Sci 2003, 87, 2083.
30. Harrats, C.; Dedecker, K.; Groeninckx, G.; Jerôme, R. Macromol Symp 2003, 198, 183.
31. Rol, R. T.; Groeninckx, G., Vinckier, I.; Moldenaers, P.; Mewis, J. Polymer 2004, 45, 2587.
32. Martin, P.; Maquet, C.; Legras, R.; Bailly, C.; Leemans, L.; van Grup, M.; vaan Duin, M. Polymer 2004, 45, 3277.
33. Jose, S.; Thomas, S.; Lievana, E.; Karger-Kocsis, J. J Appl Polym Sci 2005, 95, 1376.
34. Hoffman, J. D.; Davis, G. T.; Lauritzen, J. I. In Treatise on Solid State Chemistry; Hannay, N. B., Ed.; Plenum: New York, 1976.
35. Bassett, D. C. Principles of Polymer Morphology; Cambridge University Press: New York, 1981.
36. Cascone, E.; David, D. J.; Lorenzo, M. L. D.; Karasz, F. E.; Macknight, W. J.; Martusceelli, E.; Raimo, M. J Appl Polym Sci 2001, 82, 2934.
37. Sabino, M. A.; Feijoo. J. L.; Muller, A. J. Macromol Chem Phys 2000, 201, 2687.
38. Jang, G. S.; Jo, N. J.; Cho, W. J.; Ha, C. S. J Appl Polym Sci 2002, 83, 201.
39. Magill, J. H. Polymer 1962, 3, 655.
40. Magill, J. H. Crystallization of Polyamides II. Nylon 6 and Nylon 66; Mellon Institute: Pittsburgh, PA, 1965; pp 6 and 367.
41. Shalaby, S. W. In Thermal Characterisation of Polymeric Materials; Turi, E. A., Ed.; Academic: Orlando, FL, 1981.
42. Martuscelli, E.; Pracella, M.; Wang, P. Y. Polymer 1984, 25, 1097.
43. Van Krevelen, D. W. Properties of Polymers; Elsevier Science: Amsterdam, 1990.
44. Richardson, P. H.; Richards, R. W.; Blundell, D. J.; Mac Donald, W. A.; Mills, P. Polymer 1995, 36, 3059.
45. Bicerano, J. J Macromol Sci Rev Macromol Chem Phys 1998, 1, 391.
46. Li, J.; Shanks, R. A.; Long. Y. J Appl Polym Sci 2001, 82, 628.
47. Da Silva, A. L. N.; Rocha, M. C. G.; Lopes, L.; Chagas, B. S.; Coutinho, F. M. B. J Appl Polym Sci 2001, 81, 3530.
48. Mark, J. E. Physical Properties of Polymers Hand Book; American Institutes of Physics: Woodbury, NY, 1996.
49. Lorenzo, M. D. L. Prog Polym Sci 2003, 28, 663.
50. Mareau, V. H.; Prud'homme, R. E. Macromolecules 2002, 35, 5338.
51. Mareau, V. H.; Prud'homme, R. E. Macromolecules 2005, 38, 398.
52. George, S.; Joseph, R.; Thomas, S.; Varughese, K. T. Polymer 1995, 23, 4405.
53. George, S.; Neelakantan, N. R.; Varughese, K. T.; Thomas, S. J Polym Sci Part B: Polym Phys 1997, 35, 2309.
54. Dai, P.S.; Cebe, P.; Capel, M. Polymer 2002, 40, 1644.
55. Ana Lucia, N.; Da Silva, M. C. G. R.; Lopes, L.; Chagas, B. S.; Coutinho, F. M. B. J Appl Polym Sci 2001, 81, 3530.
56. Martuscelli, E. Polym Eng Sci 1984, 24, 563.
57. Martuscelli, E.; Silvestre, C.; Bianchi, L. Polymer 1983, 24, 1458.
58. Bartczak, Z.; Galeski, A.; Martuscelli, E. Polym Eng Sci 1984, 24, 1458.
59. Caldas, V.; Brown, G. R.; Wills, J. M. Macromolecules 1990, 1, 338.
60. Saito, C. P.; Inoue, T.; Eber, M.; Koch, E. Macromolecules 1998; 31; 4963.